The Effects of Cloud Detrainment on the Diagnosed Properties of Cumulus Populations

RICHARD H. JOHNSON

National Hurricane and Experimental Meteorology Laboratory, NOAA, Coral Gables, Fla. 33124

(Manuscript received 29 July 1976, in revised form 1 November 1976)

ABSTRACT

Lateral detrainment from cumulus updrafts and its effect on the properties of cumulus cloud populations (as determined from large-scale observations) are examined. This detrainment, which can be related to the cumulus life cycle, has been specified for a spectrum of cloud sizes by considering initially the character of detrainment for the two extremes of convection: deep cumulonimbi and shallow cumuli. The main purpose is to determine for some reasonable assumption of individual cloud detrainment to what extent diagnosed cloud ensemble properties differ from those given by applying a steady-state plume model for convective updrafts and downdrafts.

Application of the model to tropical western Pacific data indicates, as earlier studies have shown, that in convectively disturbed situations a bimodal cloud population exists of predominantly deep and shallow cumuli. However, the contribution to the total cloud-base mass flux from deep cumuli is increased and from shallow cumuli decreased somewhat when the effects of lateral detrainment are taken into account. Convective downdrafts maintained by precipitation evaporation are found to contribute in an important way to the total convective mass flux regardless of whether side detrainment from updrafts is included or not.

1. Introduction

Several methods have been recently developed that use synoptic-scale meteorological observations and simple cloud models to diagnose the interactions between cumulus convection and the large-scale atmospheric circulation (Yanai *et al.*, 1973; Ogura and Cho, 1973; Nitta, 1975). These studies support the concept that convective modification of the large-scale temperature and moisture stratification arises from an imbalance between two opposing effects: warming, drying in response to cumulus-induced subsidence in the between-cloud environment and cooling, moistening due to evaporation of detrained liquid water and detrainment of water vapor from cumulus updrafts.

It should be emphasized, however, that quantitative results from diagnostic studies of this type are to a large extent cloud-model dependent. Initial efforts have modeled the cumulus cloud as a one-dimensional, steady-state, entraining plume updraft with detrainment occurring only at cloud top. More realistically, detrainment of cloud properties takes place throughout the depth and life cycle of individual cumulus clouds. Kuo (1965, 1974), Fraedrich (1973, 1974) and Betts (1975) have discussed the effects of lateral mixing or continuous detrainment over cloud life cycles on the large-scale thermodynamic stratification. Soong and Ogura (1976), using an axisymmetric time-dependent cloud model, determined the heating and moisturizing effects of individual cloud during their whole lifetimes. They applied these results together with the large-scale heat and moisture budgets during an undisturbed period of BOMEX to diagnose the number of each type of cloud per unit area and the cloud area coverage. Recently, Fraedrich (1976), using direct observations of the number and area coverage of clouds in an undisturbed trade wind situation in Florida, determined the vertical mass flux, lateral detrainment and final detrainment for a model ensemble of transient cumulus clouds. He found lateral detrainment, not cloud top detrainment, to be the dominant detrainment mechanism for the shallow cloud population that was studied.

A number of observational investigations of cumulus clouds have shown that at least during a portion of the cumulus life cycle convective downdrafts have mass, heat and moisture transports comparable in magnitude to those in the updraft (e.g., Braham, 1952; Malkus, 1955; Betts, 1973). When averaged over the cloud life cycle these downdraft transports are likely to still be relatively important. Using one-dimensional plume models for both cumulus updrafts and downdrafts Johnson (1976) has developed a diagnostic method to determine the contributions by updrafts and downdrafts to the total convective transport. Application of this method to data taken within tropical disturbances shows that downdrafts cannot be neglected in the determination of the mass, heat and moisture budgets during periods of deep convective activity. This finding is supported by Cho (1977) who has recently developed a theory for diagnosing convective transports that explicitly takes into account the life cycles of cumulus clouds.

The modeling of updrafts and downdrafts as steady-state entraining plumes, however, does not permit the process of cloud detrainment to be realistically represented. In this paper we will examine the effects of detrainment from the sides of clouds during their life cycle. By relating updraft detrainment to updraft entrainment it is shown that mass flux and detrainment characteristics of cloud populations can be determined. Comparison of diagnosed properties of cumulus clouds populations using both the entraining plume model and cloud model with side detrainment will be stressed.

2. Diagnostic model

a. Integral equation for $m_B(\lambda)$ using general cloud model

The treatment of this problem is based on the theory of Arakawa and Schubert (1974) as it has been applied to the diagnosis of properties of cloud populations using large-scale observations (Ogura and Cho, 1973; Nitta, 1975). Cumulus convection is explicitly represented in terms of a spectrum of cloud sizes by means of an entrainment parameter λ. The total convective mass flux is distributed among cloud updrafts (entraining plumes) of different sizes in a manner determined by the cloud-base mass flux distribution function $m_B(\lambda)$. A modification of this diagnostic theory by Johnson (1976) to include effects of cumulus-scale downdrafts retains the specification of cloud size in terms of λ. The following development omits a number of details in this theory that can be found in the above papers.

We will consider a model for the cumulus updraft that includes entrainment and detrainment throughout the entire cloud depth. Furthermore, the assumption will be made that significant detrainment occurs from deep cumulonimbi in a thin layer at cloud top (as in the case of cumulonimbus cirrus shields or anvils). Final detrainment from shallow cumulus updrafts is probably less concentrated at cloud top and will receive special attention. Convective downdrafts will be modeled as in Johnson (1976) as entraining plumes with detrainment occurring only below cloud base. We assume that each updraft has a corresponding downdraft extending from some level below cloud top to the subcloud layer.

We denote $m_{ui}(\lambda,p)d\lambda$ as the entrained mass flux and $m_u(\lambda,p)d\lambda$ as the total mass flux within updrafts having entrainment rates in the interval $(\lambda, \lambda+d\lambda)$ at pressure p. The entrainment rate constant λ (Arakawa and Schubert, 1974) is defined by

$$\frac{1}{m_u(\lambda,p)}\frac{\partial}{\partial p}m_{ui}(\lambda,p)=\frac{-\lambda H}{p}, \tag{1}$$

where $H\equiv RT_v/g$, R is the gas constant for dry air, T_v the virtual temperature and g the acceleration of gravity. Similarly, for downdrafts

$$\frac{1}{m_d(\lambda,p)}\frac{\partial}{\partial p}m_{di}(\lambda,p)=\frac{\lambda H}{p}. \tag{2}$$

The updraft mass flux m_u and downdraft mass flux m_d are defined as positive and negative quantities, respectively. The thermodynamic properties of updrafts (downdrafts) are determined by moist adiabatic ascent (descent) modified by entrainment:

$$\frac{\partial h_u(\lambda,p)}{\partial p}=\frac{\xi_u(\lambda,p)}{m_u(\lambda,p)}[h_u(\lambda,p)-\tilde{h}(p)], \tag{3}$$

$$\frac{\partial h_d(\lambda,p)}{\partial p}=\frac{\xi_d(\lambda,p)}{m_d(\lambda,p)}[h_d(\lambda,p)-\tilde{h}(p)], \tag{4}$$

where the moist static energy h is given by $c_pT+Lq+gz$, c_p being specific heat at constant pressure, L the latent heat of condensation, q the specific humidity and z geopotential height; the tilde refers to values external to the cloud and $\xi_u\equiv-\partial m_{ui}/\partial p$, $\xi_d\equiv-\partial m_{di}/\partial p$. We note that detrainment does not affect thermodynamic properties within the cloud. Entrainment ξ and detrainment δ are related to the mass flux at any level by mass continuity:

$$\frac{\partial m_u(\lambda,p)}{\partial p}=\delta_u(\lambda,p)-\xi_u(\lambda,p), \tag{5}$$

$$\frac{\partial m_d(\lambda,p)}{\partial p}=\delta_d(\lambda,p)-\xi_d(\lambda,p). \tag{6}$$

In this study we neglect detrainment from downdrafts, which, as we will see, have combined mass flux less than that in updrafts in the region above cloud base; i.e., we set $\delta_d=0$. Downdraft detrainment, if included, would have only a small effect on the computed mass, heat and moisture budgets. The study by Betts (1976) of downdrafts in tropical squall lines over Venezuela indicates that some detrainment from downdrafts may occur above cloud base in a layer $\sim$100 mb deep. A similar finding has been reported for tropical western Pacific data by Johnson (1976, Fig. 1).

The moist static energy flux within a large-scale area containing numerous convective elements which occupy only a small fraction of that area is given by

$$-\overline{\omega'h'}=\int_0^{\lambda_D(p)} m_u(\lambda,p)(h_u-\tilde{h})d\lambda + \int_0^{\lambda_D(p)} m_d(\lambda,p)(h_d-\tilde{h})d\lambda, \tag{7}$$

where $\lambda_D(p)$ is the entrainment rate for clouds having their tops at p, the overbar denotes a large-scale average and the prime a deviation from that average.

Combining the heat and water vapor equations averaged over a large-scale area yields

$$Q_1-Q_2-Q_R=-\frac{\partial(\overline{h'\omega'})}{\partial p}, \tag{8}$$

where

$$Q_1 \equiv \frac{\partial \bar{s}}{\partial t} + \bar{\mathbf{v}} \cdot \nabla \bar{s} + \bar{\omega} \frac{\partial \bar{s}}{\partial p},$$

$$Q_2 \equiv -L\left(\frac{\partial \bar{q}}{\partial t} + \bar{\mathbf{v}} \cdot \nabla \bar{q} + \bar{\omega} \frac{\partial \bar{q}}{\partial p}\right),$$

$s \equiv c_p T + gz$ is the dry static energy and Q_R the horizontally averaged radiative heating rate. From Eqs. (3)–(8), we obtain

$$Q_1 - Q_2 - Q_R = -M_c \frac{\partial \tilde{h}}{\partial p} + \int_0^{\lambda_D(p)} \delta_u(\lambda,p)[h_u(\lambda,p) - \tilde{h}(p)]d\lambda + \delta^*(p)[h_u(\lambda_D,p) - \tilde{h}(p)]. \quad (9)$$

Here

$$M_c(p) = \int_0^{\lambda_D(p)} [m_u(\lambda,p) + m_d(\lambda,p)]d\lambda$$

is the net cumulus mass flux and $\delta^*(p) \equiv m_u(\lambda_D,p)d\lambda_D/dp$ represents the terminal detrainment rate for clouds with tops at p. If there is no detrainment from the sides of updrafts, $\delta_u(\lambda,p) = 0$, and (9) reduces to the familiar form given, for example, by Eq. (40) of Ogura and Cho (1973). Recalling that downdraft detrainment above cloud base has been neglected, we note that downdrafts modify the large-scale moist static energy field only through their influence on the net cumulus mass flux M_c, as indicated in the first term on the right-hand side of (9). A reduction in M_c and a consequent reduction in environmental sinking (warming, drying) in the lower troposphere over that obtained in earlier diagnostic studies (Yanai *et al.*, 1973; Ogura and Cho, 1973; Nitta, 1975) have been found by Johnson (1976) when downdraft effects have been included. Betts (1975) applied the form of (9) that results when only one cloud type is present to a study of convective transports in nonprecipitating trade wind cumuli. He specified λ and solved for the vertical distributions of the mass flux and detrainment. For convectively disturbed conditions this approach will not work since both deep and shallow cumuli are prevalent (e.g., Ogura and Cho, 1973).

b. Detrainment approximations

To solve (9) for convective transports further approximations must be made. By relating updraft detrainment to updraft entrainment through the relation

$$\delta_u(\lambda,p) = \alpha(\lambda,p)\xi_u(\lambda,p) = \alpha(\lambda,p)\frac{\lambda H}{p} m_u(\lambda,p), \quad (10)$$

we may solve (5) to obtain

$$m_u(\lambda,p) = m_B(\lambda)\eta_u(\lambda,p). \quad (11)$$

In (11) $\eta_u(\lambda,p)$ is defined by

$$\eta_u(\lambda,p) \equiv \exp\left\{\int_p^{p_B} [1-\alpha(\lambda,p)]\frac{\lambda H}{p} dp\right\}, \quad (12)$$

In the above $m_B(\lambda)$ is the cloud base mass flux distribution function and p_B the cloud base pressure. The motivation for (10) and selection of $\alpha(\lambda,p)$ will be discussed shortly. From (2) and (6) we see that

$$m_d(\lambda,p) = m_0(\lambda)\exp\left(\int_{p_0}^{p} \frac{\lambda H}{p} dp\right), \quad (13)$$

where $m_0(\lambda)$ is the downdraft originating level mass flux distribution function and $p_0(\lambda)$ the downdraft originating level. If, as in Johnson (1976), we set $m_0(\lambda)/m_B(\lambda) \equiv \epsilon(\lambda) = \text{constant}$, specify $p_0(\lambda)$ and $h_u(\lambda,p_B)$ and, furthermore, if we specify $\alpha(\lambda,p)$, then (9) may be solved for $m_B(\lambda)$.

Assumption (10) states that updraft detrainment rate is directly proportional to updraft entrainment rate and both are inversely proportional to cloud size or radius ($\lambda \propto 1/R$, where R is the cloud radius). The implication that the entrainment and detrainment rates for deep clouds (λ small) are small and for shallow clouds (λ large) are large seems reasonable. Undoubtedly, however, the ambient vertical wind shear significantly affects detrainment, as well as entrainment. Direct measurements of cumulus clouds to support the entrainment–detrainment relationship (10) are presently not available. The vertical variation of detrainment from deep cumulonimbi may differ markedly from that for shallow cumuli. It is commonly observed that cumulonimbi, in addition to side detrainment during growth and decay, detrain significantly at cloud top in the vicinity of the tropopause. To represent this variation we first consider the two extreme cases. For deep cloud updrafts we assume that mass entrainment rate ξ slightly exceeds mass detrainment rate δ below cloud top, giving an updraft mass flux increasing slowly with height, and, additionally, assume a thin detrainment layer at cloud top where the mass flux goes to zero. In the case of the shallow clouds we assume that ξ exceeds δ near cloud base, $\xi = \delta$ at midcloud level, and the mass flux decreases parabolically to near zero at cloud top. Thus, final detrainment in shallow cumuli is spread out over the upper half of the cloud depth. Clouds of intermediate sizes are assumed to have detrainment properties intermediate to these two extremes.

Normalized mass fluxes $\eta_u(\lambda,p)$, consistent with the above description, for cloud updrafts of three different sizes are presented in Fig. 1. Mass fluxes given by an entraining plume model are shown for comparison. These curves are given by (12) where for deep clouds ($\lambda \leqslant 0.125$ km^{-1})

$$\alpha(\lambda,p) = [1 + (p_B - p)/(p_B - p_D)]/2 \quad (14a)$$

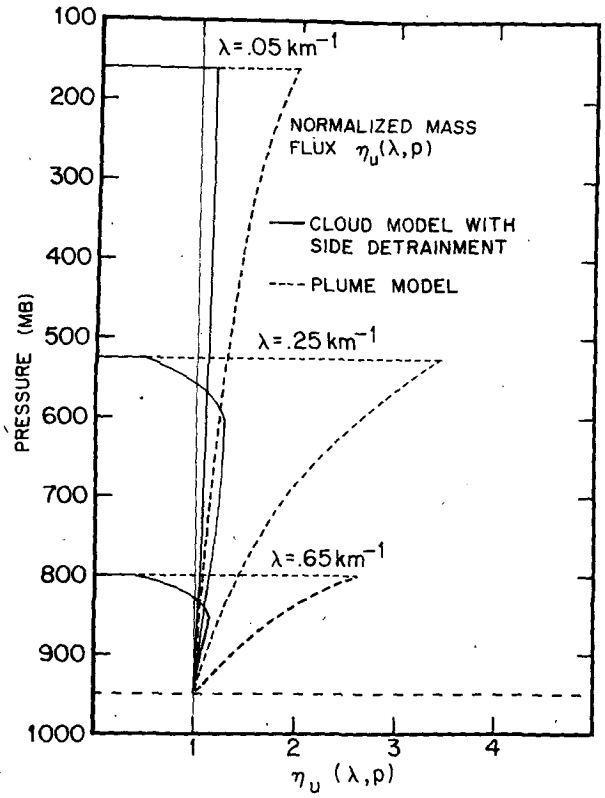

FIG. 1. Normalized mass flux $\eta_u(\lambda,p)$ for cloud model with side detrainment and plume model for clouds of three different sizes (λ=0.05, 0.25, 0.65 km^{-1}). The thin vertical line corresponds to constant mass flux profile ($\eta_u=1$).

and for all other clouds ($\lambda>0.125$ km^{-1})

$$\alpha(\lambda,p)=\begin{cases}\frac{1}{2}[1+(p_B-p)/(p_B-\hat{p})], & \hat{p}\leq p\leq p_B\\ 1-\dfrac{2p}{\lambda H}\dfrac{(p-\hat{p})}{(p_D-\hat{p}-\Delta)^2-(p-\hat{p})^2}, & p_D\leq p<\hat{p}.\end{cases} \tag{14b}$$

Here p_D is the cloud-top level, $\hat{p}$ the level where $\xi=\delta$, and Δ the pressure depth of overshooting of the zero buoyancy level at cloud top (to be discussed below); $\hat{p}$ is given by $p_B-\gamma(p_B-p_D)$, where γ increases linearly in pressure from 0.5 at $p_D=p_B$ to 1.0 at $p_D=315$ mb (corresponding to $\lambda=0.125$ km^{-1}). The fraction of the cloud depth through which the mass flux decreases parabolically to zero, determined by γ, thus ranges from half the updraft depth for the shallowest clouds down to a very small layer for clouds with tops just below 315 mb. The modeling of detrainment for the deep clouds closely resembles that of Fraedrich (1976) who assumed $\delta=\xi$ throughout cloud depth, with final detrainment in an infinitesimally thin layer at cloud top.

In order to permit a smooth transition from large cloud-top detrainment for deep clouds to small cloud-top detrainment for the shallow, we have introduced the parameter Δ. This quantity, which represents the depth of overshooting of the zero buoyancy level given by extending the parabolic profile above cloud top to $\eta_u(\lambda,\hat{p})=0$, determines the magnitude of the jump in the cloud mass flux to zero at p_D. It was desired to have $\Delta\rightarrow 0$ (no cloud-top detrainment) for the shallowest clouds. However, a nonzero Δ was found to be necessary to obtain a bounded numerical solution to (9), that is, to prevent the coefficients of $m_B[\lambda_D(p)]$, which contain $\eta_u(\lambda,p_D)$, in the system of linear algebraic equations given by the finite-difference analog of (9) (see Nitta, 1975) from vanishing. Therefore, Δ ranges from 5 mb for the shallowest clouds ($\lambda=1.8$ km^{-1}) to 25 mb for $\lambda=0.15$ km^{-1}.

Computations have been carried out for other assumptions on γ, Δ which give detrainment similar to Fig. 1 profiles, but since the mass, heat and water vapor budget results are qualitatively the same, they will not be presented in detail. The main objective is to determine to what extent the diagnosed properties of cloud populations depend on the particular cloud model that is used.

3. Convective mass flux properties and detrainment

Data used in this study are from the Reed and Recker (1971) composite of rawinsonde observations taken during the passage of a series of tropical wave disturbances through the islands of Kwajalein, Eniwetok and Ponape in the western Pacific in the summer of 1967. As in Johnson (1976), data corresponding to the mean wave trough position (the convectively active portion of the wave) are used for the analysis here. The net radiative heating rate Q_R is taken from Dopplick (1972). Yanai *et al.* (1976) have examined the effects of radiative cooling on the cloud mass flux spectrum. They discovered that the frequently found bimodal distribution of $m_B(\lambda)$ can be produced solely by typical radiative cooling rates in the tropics so long as the observed thermodynamic stratification is maintained. The large-scale vertical motion, if upward, enhances this distribution. In the presence of large-scale subsidence only a single peak corresponding to shallow clouds is found to exist. In this study, the radiative cooling, though it may be uncertain, is fixed. We are focusing attention on the influence of the cloud model itself on the distribution of $m_B(\lambda)$.

Eq. (9) has been solved for $m_B(\lambda)$ for the two cloud models described in the previous section and shown in Fig. 1. For the resolution in λ chosen (0.025 km^{-1}) six deep clouds are included in the model. Their tops are at 120, 130, 160, 190, 240 and 315 mb. We assume that the cloud virtual temperature and environmental virtual temperature are the same at cloud base and cloud top. Using Reed and Recker's mean wave trough data, $m_B(p)\equiv m_B(\lambda)d\lambda_D/dp$ has been computed for both the plume and cloud model described above. One notable

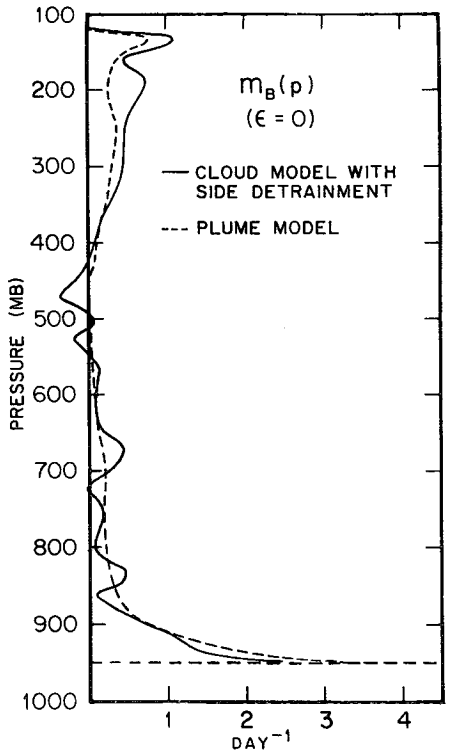

FIG. 2. Cloud-base mass flux distribution function $m_B(p)$ for cloud model with side detrainment and plume model for the no-downdraft case ($\epsilon=0$).

result (Fig. 2) is the consistent bimodal structure in $m_B(p)$ given by both models (assuming $\epsilon=0$, i.e., no downdrafts). The percent of the total cloud-base mass flux due to clouds having tops above 350 mb increases from 32 for the plume model to 49 when side detrainment effects are included. If, alternatively, we assume each cloud has a constant mass flux, namely, $\alpha(\lambda,p)=1$, then 59% of the cloud-base mass flux is due to these deep clouds. This increase is due to the smaller upper tropospheric mass flux that exists within deep updrafts of the nonplume type. To produce the same total heat transport in the upper troposphere nonplume clouds must have a greater mass flux at cloud base. Thus, we find the magnitude of $m_B(p)$ for the deep clouds to be rather sensitive to the type of cloud model that is used.

In the previous work of Johnson (1976) it was shown that the large, shallow cloud contribution to the total cloud-base mass flux is reduced considerably when the effects of convective downdrafts are included. However, we see in Fig. 2 a minor reduction in $m_B(p)$ in the lowest 100 mb unrelated to convective downdrafts. This effect is produced by the detrainment of water vapor and the evaporation of liquid water from the sides of deeper clouds. If this side detrainment is not present, as in the case of the plume model, then a larger population of shallow, moisture-determining cumuli is needed to balance the drying effect of subsidence in the between-cloud environment (see Fig. 6 later).

The function $m_B(p)$ for the nonplume cloud model contains numerous irregularities and becomes negative in several places. The extent to which the two negative departures near 500 mb affect the results at other levels below is not known. These negative values have no physical meaning and, as noted by Cho and Ogura (1974), are likely due to inaccuracies in Q_1, Q_2, Q_R or the basic thermodynamic variables, the use of an oversimplified model for the cumulus cloud, or both. The dependency of these negative values on the cloud model is clearly illustrated in the results here.

In Fig. 3 side detrainment $\int\delta_u(\lambda,p)d\lambda$ and cloud-top detrainment δ^* are shown for the nonplume cloud model for $\epsilon=0$. Note the predominant cloud-top detrainment in the upper troposphere and side detrainment from updrafts in the lower troposphere. This result is determined, in large part, by our specification of $\alpha(\lambda,p)$ in (14). Approximately 13% of the total detrainment in the lower troposphere below 500 mb is from the sides of updrafts having tops above 500 mb. The peak in δ^* near cloud base, also found by Fraedrich (1976), may not be realistic. It exists even though the assumed overshooting at this level is quite small ($\Delta\approx 5$ mb). The net detrainment, $\delta^*+\int\delta_u(\lambda,p)d\lambda$, is at most levels less than the plume model cloud-top detrainment δ. Similarly, the total entrainment into nonplume clouds

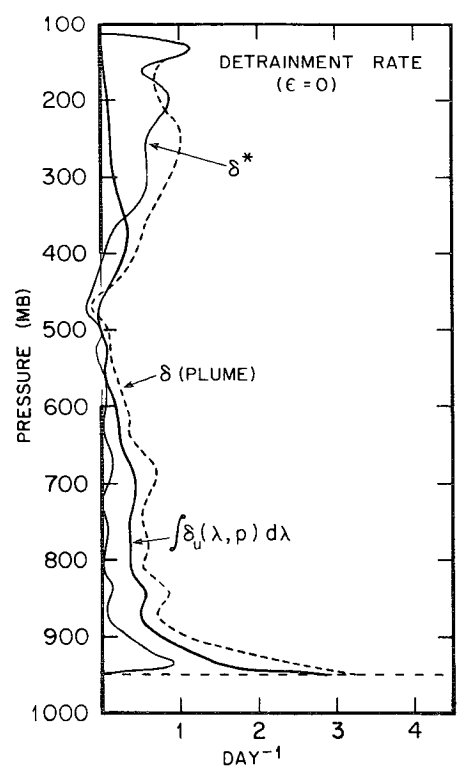

FIG. 3. Detrainment rate for plume model (δ), cloud-top detrainment rate (δ^*) and lateral detrainment rate from updrafts [$\int\delta_u(\lambda,p)d\lambda$] for cloud model with side detrainment. Downdraft effects are neglected ($\epsilon=0$).

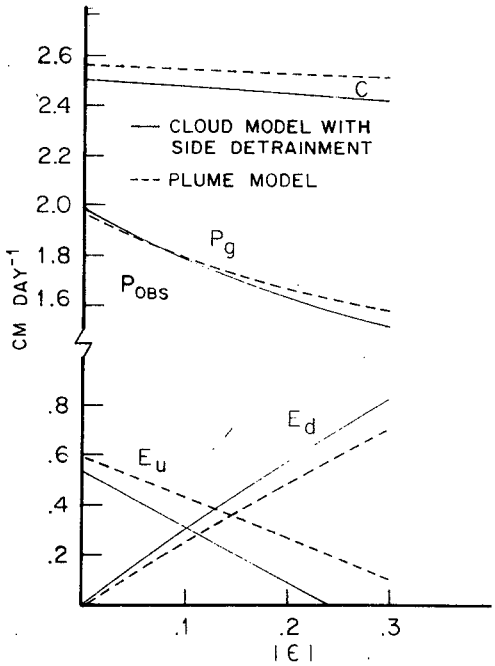

FIG. 4. Condensation rate (C), evaporation rate of detrained liquid water from updrafts (E_u), precipitation evaporation in downdrafts (E_d) and precipitation rate at the ground (P_g) as a function of $|\epsilon| \equiv |m_0(\lambda)/m_B(\lambda)|$ for cloud model with side detrainment and plume model. P_{OBS} is the observed rainfall rate for the average trough position of the Reed and Recker composite wave. The ratio of the downdraft pressure depth to the updraft pressure depth (β) is 0.75.

(not shown) is less, implying a net decrease in the total cloud-environment mass exchange.

Condensation rate C, updraft evaporation rate E_u, downdraft evaporation rate E_d (assuming a saturated downdraft) and precipitation P_g at the ground have been computed for both cloud models (Fig. 4). Precipitation evaporation in the subcloud layer is determined by assuming evaporation given by the cloud model at cloud base is constant through the subcloud layer. As in Johnson (1976) we take the pressure depth of each downdraft to be a fraction (β) equal to three-fourths the depth of its associated updraft. Regardless of which cloud model is used, we conclude from Fig. 4 that downdraft transports are important. For $|\epsilon| \approx 0.2$ -0.25 we find approximate agreement between model-computed and observed precipitation.

Updraft, downdraft and net cumulus mass fluxes for $\epsilon = -0.2$ and $\beta = 0.75$ for both cloud models are shown in Fig. 5. Between 900 and 400 mb there is a 15–20% reduction in M_c when side detrainment effects are included. This is partly due to an increase in the downdraft transport which is larger because $m_B(\lambda)$ and hence $m_0(\lambda)$ is larger for deep clouds (λ small). The reduction in M_u is a direct consequence of the reduced normalized mass flux in clouds which detrain throughout their depth in comparison to clouds modeled as entraining plumes.

The water vapor budget is presented in Fig. 6. Updraft evaporation $\bar{e}_u$ represents evaporation of detrained liquid water from the sides and tops of cumulus updrafts. It is determined as a residual in the water vapor budget equation

$$-\frac{Q_2}{L} = -M_c\frac{\partial \tilde{q}}{\partial p} + \delta^*(q_u - \tilde{q}) + \int_0^{\lambda_D(p)} \delta_u(\lambda,p)[q_u(\lambda,p) - \tilde{q}(p)]d\lambda + \bar{e}_u. \quad (15)$$

For the case of no downdrafts (Fig. 6a), $-Q_2/L$ is largely given by an imbalance between the opposing effects of environmental subsidence drying $-M_c\partial\tilde{q}/\partial p$ in response to the net cumulus mass flux and moistening due to cloud side detrainment of water vapor $\int\delta_u(q_u-\tilde{q}/d\lambda$ and evaporation of detrained liquid water $\bar{e}_u$. Cloud-top detrainment of water vapor $\delta^*(q_u-\tilde{q})$ is relatively small except near cloud base. When downdraft effects are included (Fig. 6b), both environmental subsidence drying and detrainment moistening are reduced considerably, by an amount roughly equivalent to that found in the case of the plume model (Johnson, 1976).

The effects of cloud detrainment on the heat budget have also been examined. In previous diagnostic studies

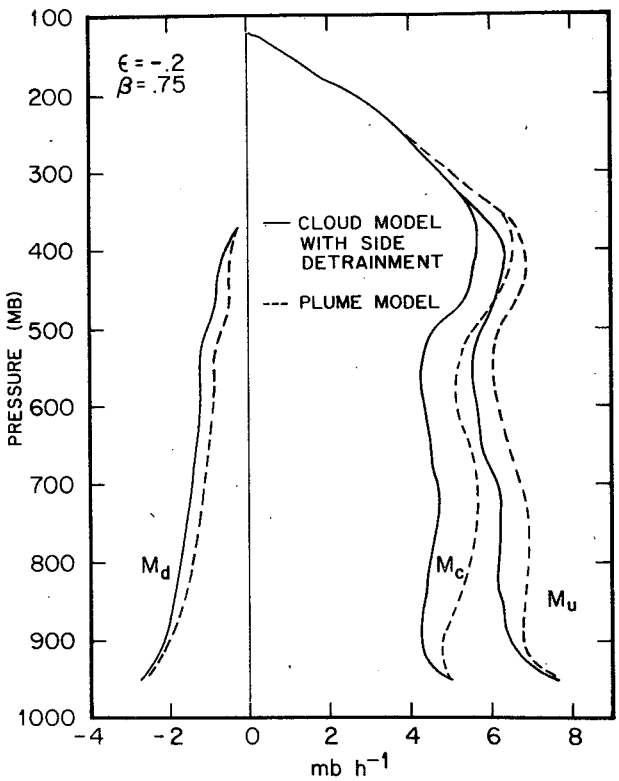

FIG. 5. Updraft mass flux M_u, downdraft mass flux M_d and net cumulus mass flux M_c for cloud model with side detrainment and plume model. Relative downdraft intensity and depth are given by $\epsilon = -0.2$, $\beta = 0.75$.

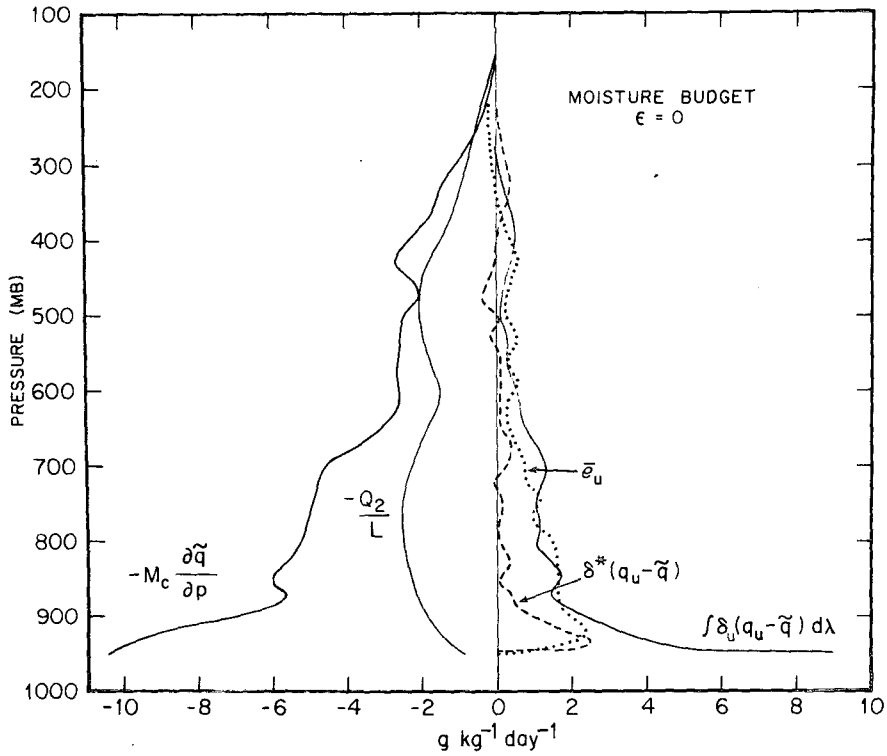

FIG. 6a. Terms in the water vapor balance equation for cloud model with side detrainment (no downdrafts, $\epsilon=0$). Q_2 is the "apparent moisture sink," $-M_c(\partial\tilde{q}/\partial p)$ is the drying due to compensating mass flux in the environment, $\bar{e}_u$ the evaporation of detrained liquid water from the sides and tops of updrafts, $\delta^*(q_u-\tilde{q})$ the cloud-top detrainment of water vapor and $\int \delta_u(q_u-\tilde{q})d\lambda$ the detrainment of water vapor from the sides of updrafts.

(Yanai *et al.*, 1973; Ogura and Cho, 1973; Nitta, 1975) it was concluded that the detrainment of heat represents a negligible contribution to the heat budget simply because the only detrainment that takes place is at cloud top, where $s_u-\tilde{s}$ is either zero (Yanai *et al.*, 1973; Ogura and Cho, 1973) or very small (Nitta, 1975). For the model developed here the detrainment of heat could conceivably be important since the effect of lateral detrainment from the sides of updrafts is included. However, computations show this effect ($\sim$0.4°C day^{-1} at 500 mb) to be at least an order of magnitude smaller than warming produced by subsidence compensating the net cumulus mass flux ($\sim$8°C day^{-1} at 500 mb). Thus, the earlier conclusion of Yanai *et al.* (1973), namely, that the dominant processes affecting the heat balance are subsidence warming compensating the cumulus mass flux and evaporation of detrained liquid water, remains essentially unchanged.

4. Summary and discussion

We have examined the effects of an important characteristic feature of the cloud life cycle, namely, lateral detrainment from cumulus updrafts, on the diagnosed properties of cumulus cloud populations. Comparison with diagnostic model computations based on a steady-state entraining plume model for the cumulus updraft reveals several interesting results. First, when the effects of cloud side detrainment are included, there is an increase in the contribution to the total cloud base mass flux from deep cumulonimbi and a decreased contribution from shallow cumuli over that obtained from the plume cloud model. The net cumulus mass flux in the mid- to lower troposphere is reduced 15–20% because of a slight decrease in the updraft mass flux and a slight increase in the magnitude of the downdraft mass flux. Second, it is found that regardless of which cloud model is used, convective downdrafts are determined to contribute importantly to the total convective mass flux. It appears as though their effects on the heat and moisture budgets are significant and will need to be included in theories for the parameterization of cumulus convection (Johnson, 1976). We have found that the neglect of convective downdrafts has a more serious effect on the diagnosed mass flux properties of cloud populations than the neglect of lateral detrainment from cumulus updrafts although the latter effects are not negligible. Our results indicate that the use of the entraining plume model for convective updrafts, where detrainment from the cumulus ensemble is crudely represented by cloud-top detrainment from a continuous distribution of cloud sizes, may be a

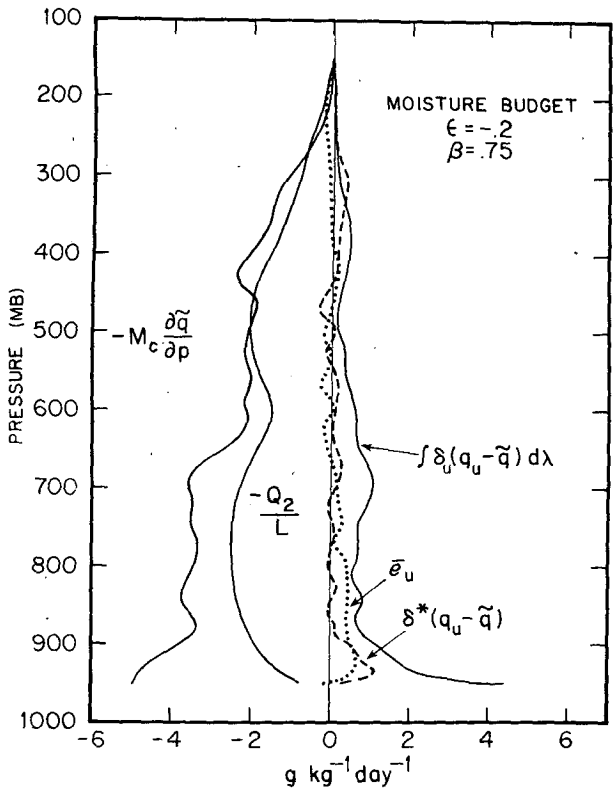

FIG. 6b. Water vapor balance for the downdraft case ($\epsilon = -0.2, \beta = 0.75$).

satisfactory approximation—as long as convective downdrafts are properly taken into account.

Since it has been necessary to specify detrainment from cumulus updrafts in order to solve for the cloud-base mass flux distribution function, there are definite limitations on the quantitative usefulness of the results presented here. One concern is that the inversion of (9) yields negative values of $m_B(\lambda)$ of appreciable size in the mid-troposphere when a cloud model is used that does not restrict detrainment from individual cumuli to an infinitesimal layer at cloud top. Certainly an improved data set, one which includes direct measurements of the net radiative heating, would be highly desirable for further application of the diagnostic model developed here. A possible improvement would be to determine $\delta_u(\lambda, p)$ from a time-dependent cloud model and then reexamine the mass, heat and water vapor transports for the cloud population.

Acknowledgments. The helpful comments of Drs. Stanley L. Rosenthal, Lloyd J. Shapiro, John M. Brown and one of the reviewers have been appreciated. Thanks are also extended to Dale Martin for drafting the figures and Helena Czarniecki and Sara Hernandez for typing the manuscript.

REFERENCES

Arakawa, A., and W. Schubert, 1974: Interaction of a cumulus cloud ensemble with the large scale environment, Part I. *J. Atmos. Sci.*, **31**, 674–701.

Betts, A. K., 1973: A composite mesoscale cumulonimbus budget. *J. Atmos. Sci.*, **30**, 597–610.

——, 1975: Parametric interpretation of trade-wind cumulus budget studies. *J. Atmos. Sci.*, **32**, 1934–1945.

——, 1976: The thermodynamic transformation of the tropical subcloud layer by precipitation and downdrafts. *J. Atmos. Sci.*, **33**, 1008–1020.

Braham, R. R., 1952: The water and energy budgets of the thunderstorm and their relation to thunderstorm development. *J. Meteor.*, **9**, 227–242.

Cho, H. R., 1977: Contributions of cumulus cloud life-cycle effects to the large-scale heat and moisture budget equations. *J. Atmos. Sci.*, **34**, 87–97.

——, and Y. Ogura, 1974: A relationship between cloud activity and low-level convergence as observed in Reed-Recker's composite easterly waves. *J. Atmos. Sci.*, **31**, 2058–2065.

Dopplick, T. G., 1972: Radiative heating of the global atmosphere. *J. Atmos. Sci.*, **29**, 1278–1294.

Fraedrich, K., 1973: On the parameterization of cumulus convection by lateral mixing and compensating subsidence, Part I. *J. Atmos. Sci.*, **30**, 408–413.

——, 1974: Dynamic and thermodynamic aspects of the parameterization of cumulus convection, Part II. *J. Atmos. Sci.*, **31**, 1838–1849.

——, 1976: A mass budget of an ensemble of transient cumulus clouds determined from direct cloud observations. *J. Atmos. Sci.*, **33**, 262–268.

Johnson, R. H., 1976: The role of convective-scale precipitation downdrafts in cumulus and synoptic-scale interactions. *J. Atmos. Sci.*, **33**, 1890–1910.

Kuo, H. L., 1965: On the formation and intensification of tropical cyclones through latent heat release by cumulus convection. *J. Atmos. Sci.*, **22**, 40–63.

——, 1974: Further studies of the parameterization of the Influence of cumulus convection on the large scale flow. *J. Atmos. Sci.*, **31**, 1232–1240.

Malkus, J. S., 1955: On the formation and structure of downdrafts in cumulus clouds. *J. Meteor.*, **12**, 350–354.

Nitta, T., 1975: Observational determination of cloud mass flux distributions. *J. Atmos. Sci.*, **32**, 73–87.

Ogura, Y., and H. R. Cho, 1973: Diagnostic determination of cumulus cloud populations from large scale variables. *J. Atmos. Sci.*, **30**, 1276–1286.

Reed, R. J., and E. E. Recker, 1971: Structure and properties of synoptic-scale wave disturbances in the equatorial western Pacific. *J. Atmos. Sci.*, **28**, 1117–1133.

Soong, S. T., and Y. Ogura, 1976: A determination of the trade wind cumuli population using BOMEX data and an axisymmetric cloud model. *J. Atmos. Sci.*, **33**, 992–1007.

Yanai, M., S. Esbensen and J.-H. Chu, 1973: Determination of bulk properties of tropical cloud clusters from large scale heat and moisture budgets. *J. Atmos. Sci.*, **30**, 611–627.

——, J.-H. Chu, T. E. Stark and T. Nitta, 1976: Response of deep and shallow tropical maritime cumuli to large-scale processes. *J. Atmos. Sci.*, **33**, 976–991.